Polym. Bull. (2015) 72:3305–3324
DOI 10.1007/s00289-015-1467-4

ORIGINAL PAPER

Dynamic rheological studies and applicability of time–temperature superposition principle for PA12/SEBS-*g*-MA blends

Khushboo Rinawa[1] · S. N. Maiti[1] · R. Sonnier[2] · J.-M. Lopez Cuesta[2]

Received: 21 January 2015 / Revised: 18 June 2015 / Accepted: 13 July 2015 /
Published online: 2 August 2015

Abstract The viscoelastic behaviour of PA12/SEBS-*g*-MA blends was studied. Time sweep, amplitude sweep, and frequency sweep tests were analysed by the use of parallel-plate rheometer. Time sweep test shows time-independent viscoelastic behaviour of the polymer and blends during the entire duration of test. The critical shear strain was higher for PA12 as compared to that of SEBS-*g*-MA and the blends in amplitude sweep test. However, the plateau modulus was higher for SEBS-*g*-MA as compared to PA12. The complex viscosity, dynamic storage, and loss moduli of PA12 increased with the addition of SEBS-*g*-MA as a consequence of phase interaction between them. The influence of phase morphology of blend composition on their rheological properties was also examined. The blend showed a transformation from liquid-like to solid-like behaviour. The decrease in viscosity for PA12 and blends was observed with increasing temperature. The van Gurp plots was successfully used to validate time–temperature superposition principle (TTS) for PA12, SEBS-*g*-MA and blend compositions. PA12 holds TTS with a horizontal shift factor that fits Arrhenius equation. Whereas TTS fails for SEBS-*g*-MA and the blends studied because of different temperature-sensitive response and microstructural changes of melt during shear application.

Keywords Time–temperature superposition principle · Transition kinetics from solid-like to liquid-like behaviour · Dynamic rheology · PA12

✉ S. N. Maiti
maitisn49@yahoo.co.in

[1] Centre for Polymer Science and Engineering, Indian Institute of Technology Delhi, Hauz Khas, New Delhi 110016, India

[2] Centre des Matériaux de Grande Diffusion, Ecole des Mines d'Alès, 6, Avenue de Clavières, 30318 Alès Cedex, France

Introduction

Polymer blends are developed to achieve modified properties of polymers to make them useful in versatile engineering applications [1–3]. Most of the polymers are incompatible with each other. Introduction of some functionality in the polymers is the most useful and easiest route to enhance the phase interaction or compatibility between the components of a blend [4, 5]. In general, functionalized elastomers are blended with the engineering thermoplastics to acquire high toughness and good mechanical properties. Nowadays nylons with long aliphatic chains, e.g. nylon 66, nylon 11, nylon 12, and nylon 1212, are extensively applicable in automobile, electrical and electronic, cable industries because of their superior properties [6, 7]. Extensive research work related to mechanical and morphological behaviour of nylon/elastomer blends have been reported [8–10]. To our knowledge, there has been very little study on rheological properties of these blends [11, 12].

The study of deformation and melt flow behaviour of the polymer blends is very important to optimize and control the processability like extrusion, injection moulding, and film blowing operations on the material [13]. The rheological properties of polymer blends give much useful information for understanding the structure–property relationship as it is very responsive to the microstructure and phase morphology of the blends [14]. It is well established that the nature, composition, size of dispersed domain, interaction between components of the blend, and type of copolymerization affect the rheological behaviour of the blends [15]. The linear viscoelastic behaviour of the blends is of significant interest for the design and development of polymer blends [7, 16–21].

The dependence of rheological properties of blend on temperature is an important study to evaluate the actual serviceability and to explore larger time region at a definite temperature for the studied materials, given by well-known procedure called time–temperature superposition (TTS) principle. TTS was first proposed by Lenderman in 1943 [22]. William et al. [23] and Seitz et al. [24] subsequently proposed equations for semicrystalline polymers. TTS can also be used to evaluate polymer branching, homogeneity, miscibility, and phase separation in polymer blends. It has been established that TTS holds when exact superposition of shapes of adjacent rheological curves is obtained through horizontal and/or vertical shifts [25]. In general, TTS fails for polymer blends because of different temperature-dependent relaxation mechanisms for each component of the blends. However, it has been reported that TTS still holds for many blends [13, 15]. This could be achievable by increased compatibilization which generates strong phase interactions between blend components which in turn can result in single temperature dependence.

The dynamic rheological behaviour of PA12/SEBS-*g*-MA blends with different SEBS-*g*-MA concentrations is presented in this paper. The relationship between rheological properties and morphology of blends was also evaluated. The influence of temperature on rheology and applicability of TTS for these blends were analysed according to the new extended approach given by van Gurp–Palmen analysis [26].

Experimental

Materials

The PA12, VESTAMID L2140, with melt flow index of 36 cm^3/10 min (275 °C, 5.0 kg load) and density of 1.01 g/cm^3 was obtained from Evonik Degussa High-Performance Polymers. The maleated SEBS-*g*-MA copolymer was procured from Kraton Polymers (Kraton FG1901X) having 1.4–2.0 % MA content and MFI of 22 g/10 min (230 °C, 5.0 kg load) [27].

Preparation of the samples

PA12 and SEBS-*g*-MA copolymers were dried in vacuum oven at 80 °C for 18 h and 12 h, respectively. A co-rotating twin-screw extruder, Clextral, 900 mm (L/D = 42) was used to prepare binary blends of PA12/SEBS-*g*-MA at different concentration of SEBS-*g*-MA (10–50 wt%) at 220–240 °C temperature and a screw speed of 300 rpm. The extruded strands leaving the extruder die were cooled by passing through water and then granulated. The standard tensile test bars with 4 mm thickness were prepared on an injection moulding machine (Krauss Maffei -CX series) according to ISO 3167 test procedure. The melt and mould temperatures were maintained at 220–240 °C and 40 °C, respectively. The blends were named as N12, NS10, NS20, NS35, and NS50 containing 0, 10, 20, 35 and 50 wt% of SEBS-*g*-MA copolymer.

Measurements

An ARES rheometer (Advanced Scientific Expansion System) which works in parallel-plate oscillatory mode was used to perform rheological tests of melt. To determine linear viscoelastic region, dynamic strain sweep test was conducted in the range of 0.01–100 % strain at a definite frequency (1 rad/s). The change in rheological properties with frequency was noted from dynamic frequency sweep test performed in the range of 0.1–100 rad/s at 220 °C with predetermined strain amplitude of 3 %. Three different temperatures (220, 210, and 240 °C) were selected for performing dynamic frequency sweep test. The result obtained such as complex modulus (η^*), storage modulus (G'), and phase angle (δ) are used to generated isothermal curves to evaluate the TTS principle.

Results and discussion

Time sweep

A dynamic time sweep rheological experiment is the preliminary requirement to ensure melt stability during period of experiment. The time dependence of complex viscosities (η^*) of PA12, SEBS-*g*-MA, and PA12/SEBS-*g*-MA blends with 10, 20,

50 wt% of SEBS-*g*-MA over a period of 10 min at 220 °C and 1 Hz frequency is presented in Fig. 1. All the compositions are stable in the entire experimental period as η^* is invariable with time. The time-independent viscoelastic behaviour of all the samples showed no chemical alteration or structural change during the test.

Amplitude sweep

Determination of linear viscoelastic region (LVR) is required before beginning frequency sweep test to confirm the stability of microstructure of the sample under shear environment. The change in the rheological properties with increasing oscillatory strain amplitude was obtained at a definite frequency to evaluate the effect of shear strain on viscoelastic behaviour. In the linear region where plateau is observed, the applied deformation is not sufficient to affect the microstructure of the blend whereas increasing strain amplitude start disturbing the microstructure. This has decreased the storage and loss moduli after a critical amplitude value as a result of alignment of polymer chains in the shear flow direction.

Figure 2a, b represents the effect of shear strain on the dynamic storage (G') and loss (G'') moduli for PA12, SEBS-*g*-MA, and PA12/SEBS-*g*-MA blends at 220 °C and 1 Hz frequency. There was a little instability in the initial stages of the G' curve for N12 which was due to strain–torque relationship that was close to the limit of instrument sensitivity. It was observed that both G' and G'' for N12 and NS10 show linearity with strain up to 100 %, whereas NS20 and NS50 exhibit strain-independent behaviour up to 10 % strain. The elastomer SEBS-*g*-MA shows a transition from linear to nonlinear regime at about 5 % strain. Thus, further rheological characterizations were performed at 3 % strain amplitude value. In the linear region, the plateau is an indication of dynamic equilibrium between disentanglement and entanglement due to lower strain value. At higher strain, the alignment and the macromolecular chain slippage have modified the microstructure

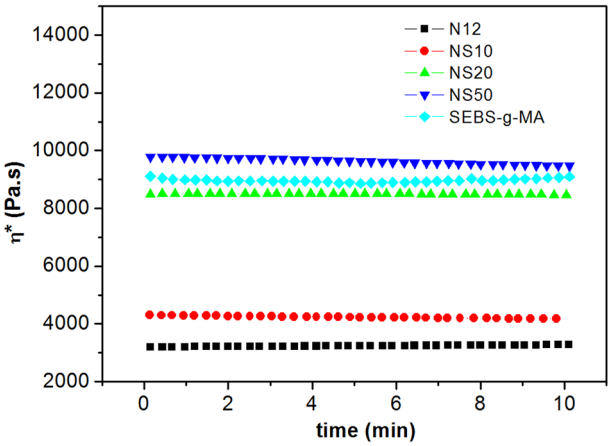

Fig. 1 Complex viscosity (η^*) as a function of time for PA12, SEBS-*g*-MA and PA12/SEBS-*g*-MA blends

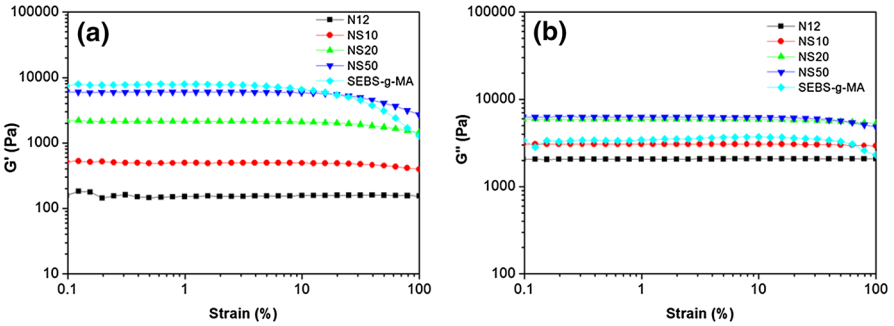

Fig. 2 Linear viscoelastic region of PA12, SEBS-*g*-MA and PA12/SEBS-*g*-MA blends based on **a** storage modulus G', and **b** loss modulus G''

which is responsible for sudden decrease in G'. It can be noted that G' is much more sensitive to strain than G'' as greater reduction was observed with G' with strain. Results show $G'' > G'$ for N12, the viscous behaviour dominates the elastic one and the material shows a liquid-like behaviour. On the contrary, $G' > G''$ for SEBS-*g*-MA, indicating dominance of elastic behaviour over viscous one and the material is semisolid in stage. The lower value of critical strain (about 5 %) for SEBS-*g*-MA demonstrated its higher sensitivity to shear strain as a consequence of its microstructure which consists of phase-separated heterogeneous moieties that can easily be destroyed by shear application. The moduli of blends were greater than that of N12 as a result of addition of high modulus elastomer.

Frequency sweep

The change in the rheological properties with increasing frequency (0.1–100 rad/s) was evaluated from dynamic sweep test. The test was conducted at 3 % strain amplitude and at 220 °C temperature to maintain the linear viscoelastic region during the experiment.

Complex viscosity (η)*

The variations in the complex viscosity ($\eta^* = \eta' - i\eta''$) with frequency at 220 °C for PA12, SEBS-*g*-MA, and PA12/SEBS-*g*-MA blends with varying amounts of elastomer are shown in Fig. 3. PA12 displays pseudo-Newtonian behaviour at low frequencies followed by shear thinning behaviour at high frequencies. SEBS-*g*-MA copolymer shows higher viscosity and a strong shear thinning behaviour over the entire range of frequency. Addition of SEBS-*g*-MA copolymer to PA12 matrix has significantly increased the viscosity of the PA12 matrix. In fact, at high frequency, the viscosity of the blends is higher than both the neat polymers. The flow curves (complex viscosity vs. shear rate) were analysed according to power law model, Eq. (1):

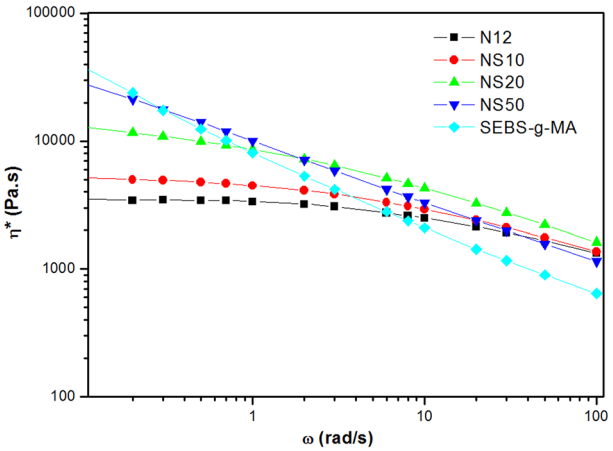

Fig. 3 Complex viscosity as a function of frequency for PA12, SEBS-*g*-MA and PA12/SEBS-*g*-MA blends with 10, 20, 50 wt% of SEBS-*g*-MA

$$\eta^* = A\omega^{n-1}, \tag{1}$$

where A is a sample specific pre-exponential factor; ω is the oscillation frequency; and n is the shear thinning exponent. A plot of log (η*) vs. log (ω) gives a straight line to determine value of n. The most fitted Carreau model, using TA Orchestrator software ($r^2 > 0.999$), was also employed to show the non-Newtonian behaviour of the blend according to Eq. (2) [28]:

$$\eta^* = c_1(1 + (c_2x)^{c_3})^{(c_4-1)/c_3}, \tag{2}$$

where c_1, c_2, c_3 and c_4 are constants. Here c_1 denotes the zero viscosity η_0.

The values of power law index (n) and zero shear viscosity (η_0) of PA12/SEBS-*g*-MA blends are given in Table 1. The value of n is less than unity and decreases with increasing elastomer concentration indicating pseudo-plastic behaviour of the polymer blends. The shear thinning behaviour of blends also increased with increasing concentration of SEBS-*g*-MA. The values of n indicate that PA12/SEBS-*g*-MA blends with 20 and 50 wt% of SEBS-*g*-MA exhibit a relatively stronger shear

Table 1 Power law index and zero viscosity from Carreau model for N12, NS10, NS20, NS50, and SEBS-*g*-MA blends

Sample	Power law index (n)	Carreau model			
		η_0 (10^4) (Pa.s)	c_2	c_3	c_4
N12	0.95	0.34	0.16	0.93	0.66
NS10	0.88	0.54	0.16	0.64	0.54
NS20	0.66	2.40	1.10	0.34	0.43
NS50	0.40	6.50	133.00	1.11	0.52
SEBS-*g*-MA	0.40	17.00	598.39	0.22	0.28

thinning effect in comparison to NS10. This is due to the fact that at low frequencies, degree of entanglement of polymeric chains dominates the flow whereas at high frequencies alignment in flow direction dominates which facilitate the flow causing sudden decrease in melt viscosity. The zero shear viscosity increased significantly for NS20 and NS50 blends. The higher viscosity of blends was caused by the resistance offered by the formation of a graft copolymer, e.g. PA12-*g*-SEBS in the blend as well as due to the high viscosity of the SEBS-*g*-MA itself. It can be noted that the viscosity increase in NS20 is more as compared to NS10 which may be attributed to sufficient amount of grafted MA to react with polar group of PA12 which hindered the melt flow of polymer to a larger extent [29].

Storage (G') and loss (G'') moduli

The variation of storage modulus (G') and loss modulus (G'') as a function of frequency (ω) at 220 °C for PA12/SEBS-*g*-MA blends is presented in Fig. 4a, b, respectively. Both the moduli increased with frequency and the increase for neat PA12 is according to linear viscoelastic model, $G' \propto \omega^2$, $G'' \propto \omega$ at low frequency. The blends show higher moduli compared to neat PA12 but they did not show linear dependence on frequency [25]. In case of SEBS-*g*-MA, there is an existence of phase-separated system and slightly ordered structure (e.g. network, agglomerated, and skeletons) under shear environment [7, 30]. The hard polystyrene block serves as entanglement points to make network structure which resists the motion of macromolecular chains responsible for plateau in the curve (Fig. 4a). It has already been observed that there is an existence of strong interaction between the components of blends which can alter the viscoelastic behaviour of PA12 matrix. In case of NS10, the shape of curve of storage modulus is dominated by PA12 matrix but with the increase in SEBS-*g*-MA concentration, the shape of curve is quite similar to that of SEBS-*g*-MA as a result of interphase graft reaction.

The variation in loss modulus G'' for the blends shows more complex behaviour (Fig. 4b). The value of G'' increases with increasing frequency of the system. For

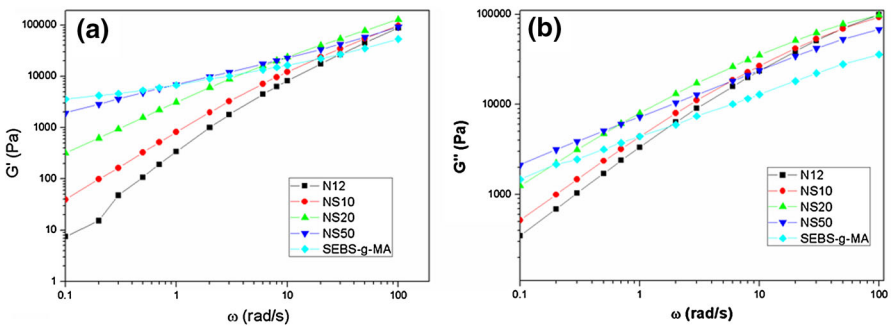

Fig. 4 **a** Storage modulus (G') and **b** loss modulus (G'') as a function of frequency for N12, SEBS-*g*-MA, and PA12/SEBS-*g*-MA blends with varying SEBS-*g*-MA content

PA12 and NS10 blend, G'' was lower than that of SEBS-*g*-MA at low-frequency region, whereas PA12 and all the blends show higher values of G'' compared to that of SEBS-*g*-MA at higher frequency region. It is already said that G' characterizes the elastic part (stored energy) and G'' gives the viscous part (energy dissipated). Thus, the elastic nature of SEBS-*g*-MA and its interaction with PA12 both have influenced the rheological parameters of the system and the greater increase in G′ as compared to G'' explicitly demonstrate the toughening behaviour of PA12/SEBS-*g*-MA blends. Significant influence of SEBS-*g*-MA on viscoelastic behaviour of PA12 was observed at low frequency where the system gets enough time for both elastic (G') and viscous (G'') part to respond to the applied stress as well as the SEBS-*g*-MA also gets loosened up. However, at higher frequency, mostly the free portion of the polymer chains can respond which is mostly unaffected by the addition of elastomer.

The shape of the rheological curve depends on several morphological parameters such as dispersed droplet size, its shape, co-continuity and the phase inversion [31]. To determine the concentration where the morphological changes govern the rheological properties, a curve between G' was plotted versus SEBS-*g*-MA concentration at different frequency (given in bracket), Fig. 5. A peak around 20 wt% of SEBS-*g*-MA in the curve at high frequency (>10 rad/s) indicated presence of microstructure changes in the blend [29]. This could be attributed to the graft reaction which significantly influenced the external stimulation. This indicates the formation of strong graft copolymer at 20 wt% of SEBS-*g*-MA in PA12 matrix as compared to other blend compositions which greatly influences the rheological properties of PA12 matrix. There was no peak in the low-frequency region of the curves but a strong transition point was seen. With further increase in SEBS-*g*-MA content, there was slight increase in the G' value at low frequency which indicates an existence of small extent of graft reaction.

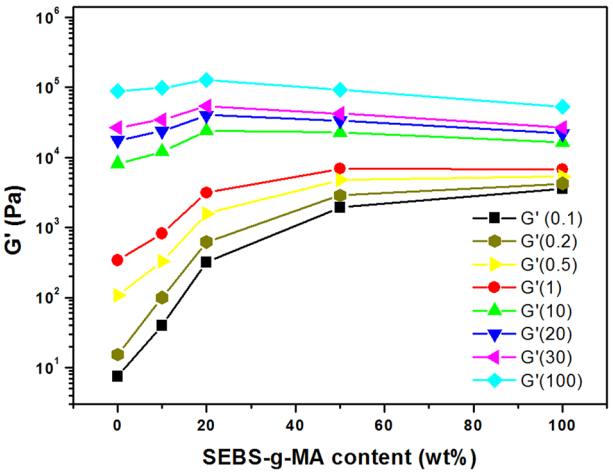

Fig. 5 Dependence of G' on the concentration of SEBS-*g*-MA for PA12/SEBS-*g*-MA blends at different frequencies

Cole–cole plot of modulus and crossover frequency

Han and coworkers used the plot of G' vs G'' (Han plots of modulus) to investigate the miscibility of blends. For compatible blends, the graph shows composition-independent correlation and for incompatible blends, composition-dependent behaviour was observed [32–34]. It can also be used to analyse the microstructural changes of the blends and polymers compatibility which give rise to an increase in G'.

Flory–Huggins interaction parameter allows assessing the interactions between two polymers to predict their miscibility according to Eq. (3) [35]:

$$(\delta_A - \delta_B)^2 = \frac{\chi_{AB} RT}{V_r}, \tag{3}$$

where χ_{AB} is the Flory–Huggins parameter, R the gas constant, T the temperature, and V_r the reference volume (100 cm^3/mol). According to the equation, the calculated value of Flory–Huggins interaction parameter χ_{AB} was found to be 7.5 (based on the solubility parameters taken from the references, PA12 = 22.2 $MPa^{1/2}$ [36], SEBS-*g*-MA = 8.5 $MPa^{1/2}$ [37]).

Flory–Huggins interaction parameter states about the miscibility of polymers but the equation does not take into account the effect of concentrations of the components on miscibility/interaction in the blend. From the interaction parameter, the blends appear immiscible, in particular, in view of the large differences between the solubility parameters of the components. However, an extent of physical interaction through hydrogen bonding and polar interactions through amide end groups of PA12 and carboxylic groups of SEBS-*g*-MA is possible [29]. This caused decrease in the globule size of the dispersed phase shown in Ref. [29].

Figure 6a presents Han plots (Cole–Cole plot of modulus) for PA12, SEBS-*g*-MA, and the blends. Although the graft reaction has improved the compatibility between the components of PA12/SEBS-*g*-MA blends but still Han plots show composition dependence of the rheological behaviour implying existence of incompatibility in the blend (Fig. 6a). This could be because of the morphological changes associated with different composition of the blends and relatively low graft ratio [29]. Figure 6a shows a straight line for N12, NS10, and NS20 blends whereas the variation of NS50 quite resembles the shape of SEBS-*g*-MA curve. The difference in the shape of curve is indication of change in melt behaviour with the incorporation of SEBS-g-MA. Also, the curves for the blends are situated left side of that of PA12 showing increased elasticity of the blends.

A transition from liquid-like to solid-like behaviour is also characterized by crossover frequency (ω_x). To determine the relaxation time, Maxwell model in dynamic mode can be used which is represented by Eq. (4):

$$\tan\delta = \frac{1}{\omega\lambda}, \tag{4}$$

where tanδ is the phase angle between G' and G'', ω the frequency of oscillation (rad/s), and λ the relaxation time (s).

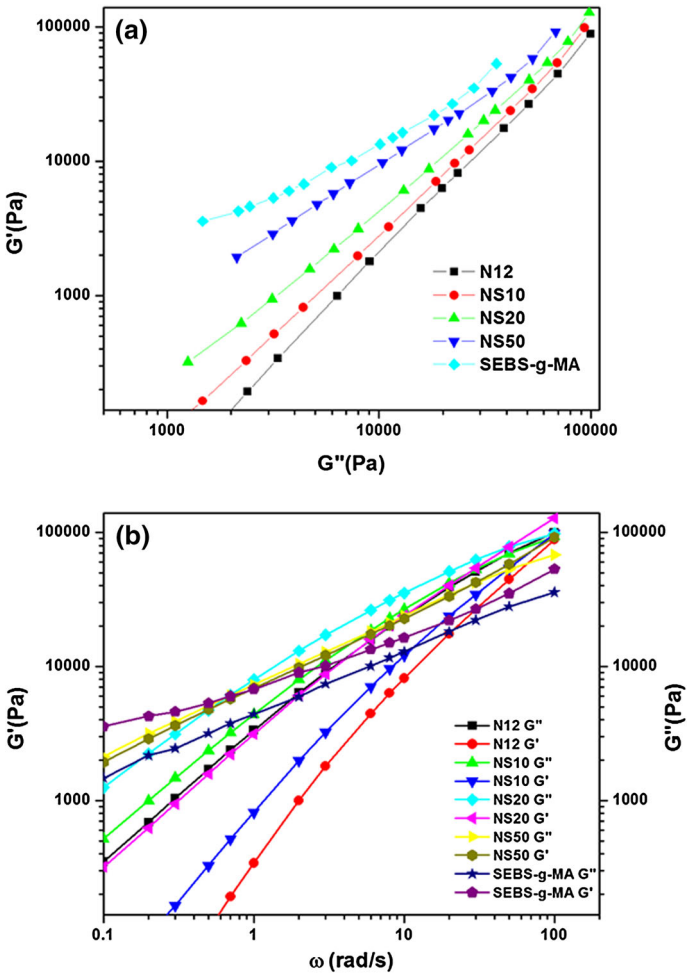

Fig. 6 Plots of **a** storage modulus (G') vs loss modulus (G''), **b** storage and loss moduli vs frequency (ω) for N12, NS10, Ns20, NS50, and SEBS-*g*-MA, respectively

At crossover, elastic and viscous components of material balance. Thus, $\tan \delta = 1$ and hence

$$\lambda = \frac{1}{\omega}. \tag{5}$$

Thus, the characteristics relaxation time (λ) of a material is the inverse of crossover frequency ω_x.

Figure 6b is used to determine crossover frequency for the samples. From Fig. 6b, the value of ω_x was 91 Hz for NS10, 53 Hz for NS20, and 29 Hz for NS50. No crossover points were detected for N12 and SEBS-*g*-MA in the studied range of ω. The value of crossover frequency decreasing with increasing concentration of SEBS-*g*-MA shows an increase in relaxation time of PA12 chains. This decrease in

repetative motion signifies pseudo-solid-like or elastic-type property of polymer system. The delay in relaxation of PA12 could be attributed to the increased graft reaction or interaction between blend components which acts as a physical barrier for the relaxation process.

The rheological data were also analysed using inverse loss tangent plots and Cole–Cole plot (between real part η' and imaginary part η'' of viscosity) as a measure of microstructural changes in polymer blend (Fig. 7a, b). Figure 7a presents plot of an inverse loss tangent versus loss modulus. PA12 shows a linear variation whereas deviation from the linearity was seen with increasing concentration of elastomer in the blends as a result of dispersed morphology. It has been reported that the smooth arc-like shape in the Cole–Cole plot is the measure of good

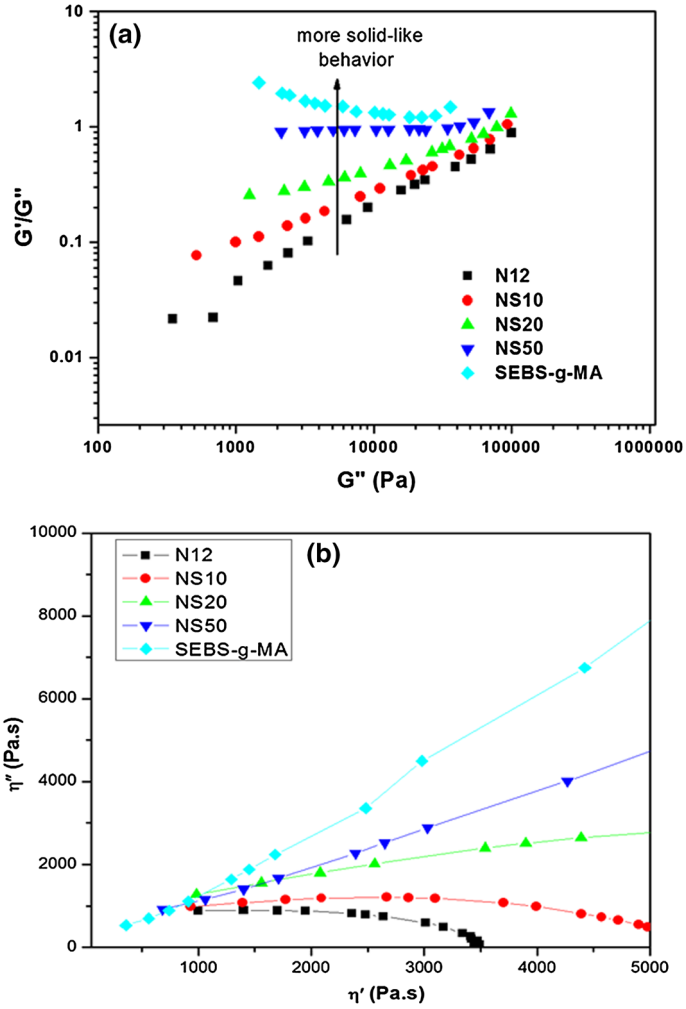

Fig. 7 Plots of **a** inverse loss tangent (G'/G'') vs loss modulus (G'), **b** Cole–Cole plot of PA12, SEBS-*g*-MA, and PA12/SEBS-*g*-MA blends

compatibility between the components [38]. The deviation from semicircular shape in the plot is a measure of solid-like behaviour of the blends (Fig. 7b). This could be due to improvement in the dispersion of elastomer particles till NS20 but still they exhibit immiscibility to some extent. In case of higher SEBS-*g*-MA content, NS50, the variation seems to be linear dominated by SEBS-*g*-MA phase (co-continuous morphology). To validate the results of Cole–Cole plots for analysing the miscibility of the blend system, van Gurp's plots were used at different temperatures showing different melt behaviour at different temperature where it can be seen that they did not merge into the common curves ("Time–temperature superposition (TTS) principle" TTS) [39].

Morphology and rheology Rheological properties of blends are very sensitive to morphological changes in the blend compositions. The morphological changes were recorded from scanning electron microscopy and the results are presented in our previous work [29]. Introduction of 10 wt% SEBS-*g*-MA to PA12 resulted in larger particles of dispersed phase as compared to NS20 which are less uniform with relatively coarse edges and relatively larger interparticle distance [29]. This indicated small extent of graft reaction due to less available MA groups. Hence, the viscoelastic behaviour of NS10 is dominated by PA12 matrix. On the other hand, 20 wt% of SEBS-*g*-MA has greatly influenced the rheology of PA12 matrix which could be attributed to the formation of smaller, uniformly dispersed particles with less interparticle distance and thus the blend entered into phase transition region. For NS50, co-continuous morphology of SEBS-*g*-MA dominated the rheology of the blend [29].

Damping behaviour The damping characteristic of a material is a measure of its efficiency to dissipate energy during molecular rearrangements and internal friction. Figure 8a shows the damping behaviour where tan δ is plotted as a function of frequency for PA12, SEBS-*g*-MA, and PA12/SEBS-*g*-MA blends. The tan δ value decreases with increasing frequency for N12, NS10, and NS20 and became flatter for NS50. SEBS-*g*-MA shows positive slope in the curve because of its solid-like behaviour (gels). At low frequency, tan δ decreases with increasing concentration of SEBS-*g*-MA elastomer as a consequence of restriction in the mobility and deformability of polymer during relaxation, raising the G' values (Fig. 6a). Also the restriction in polymer chain mobility could result in the reduced tan δ value. This decrease in tan δ values is characteristic of a polymeric system with increased relaxation time. Therefore, it can be interpreted as more solid-like or elastic behaviour of the blends. However, gelation was found by the occurrence of plateau at 50 wt% of SEBS-*g*-MA which could be attributed to the network formation of SEBS-*g*-MA and higher polymer–elastomer interaction. The van Gurp–Palmen plot (phase angle δ vs complex shear modulus) is also used to characterize the rheological response of blends (Fig. 8b) [40]. Figure 8b shows the same results and the change in the shape of the curve for NS50 blend shows the dominance of amorphous portion (SEBS-*g*-MA copolymer). The 90 degree plateau indicates elastic behaviour of the blend (NS50) [38].

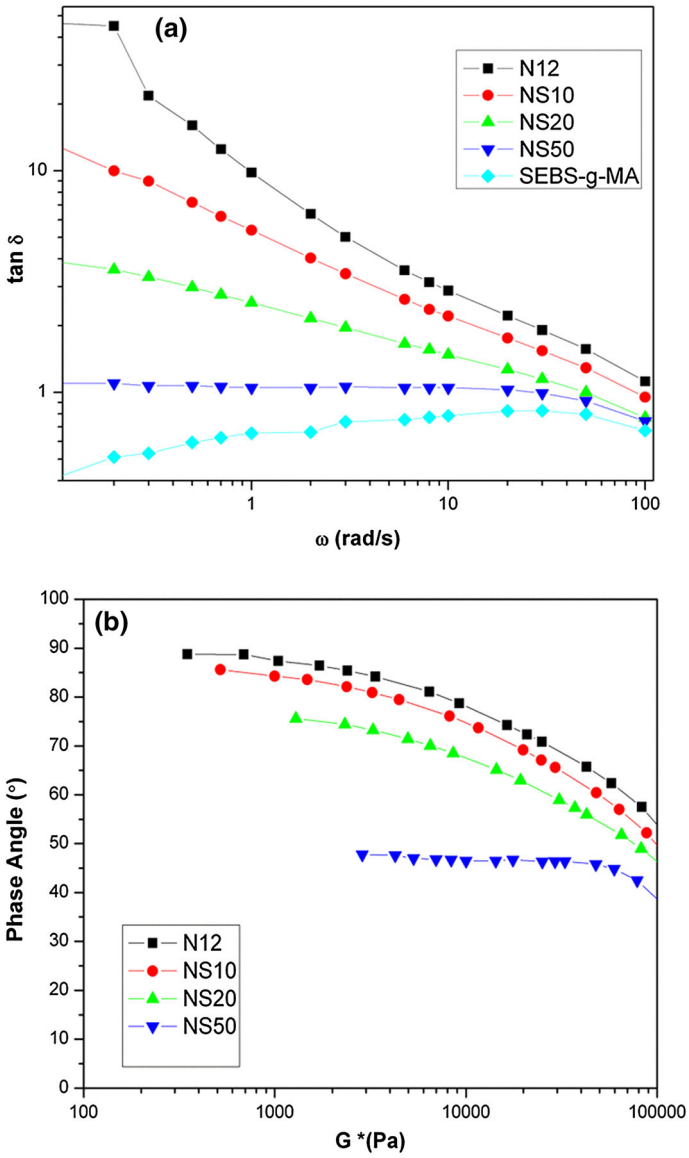

Fig. 8 Plots of **a** tan δ as a function of frequency (ω) **b** phase angle (δ) with complex modulus (G^*) for PA12, SEBS-*g*-MA, and blends

Time–temperature superposition (TTS) principle

Figure 9a–e shows the effect of temperature on viscosity of pure PA12, SEBS-*g*-MA and their blends. The viscosity decreased with increase in temperature of the system for all the samples tested. At higher temperature, the entanglements within

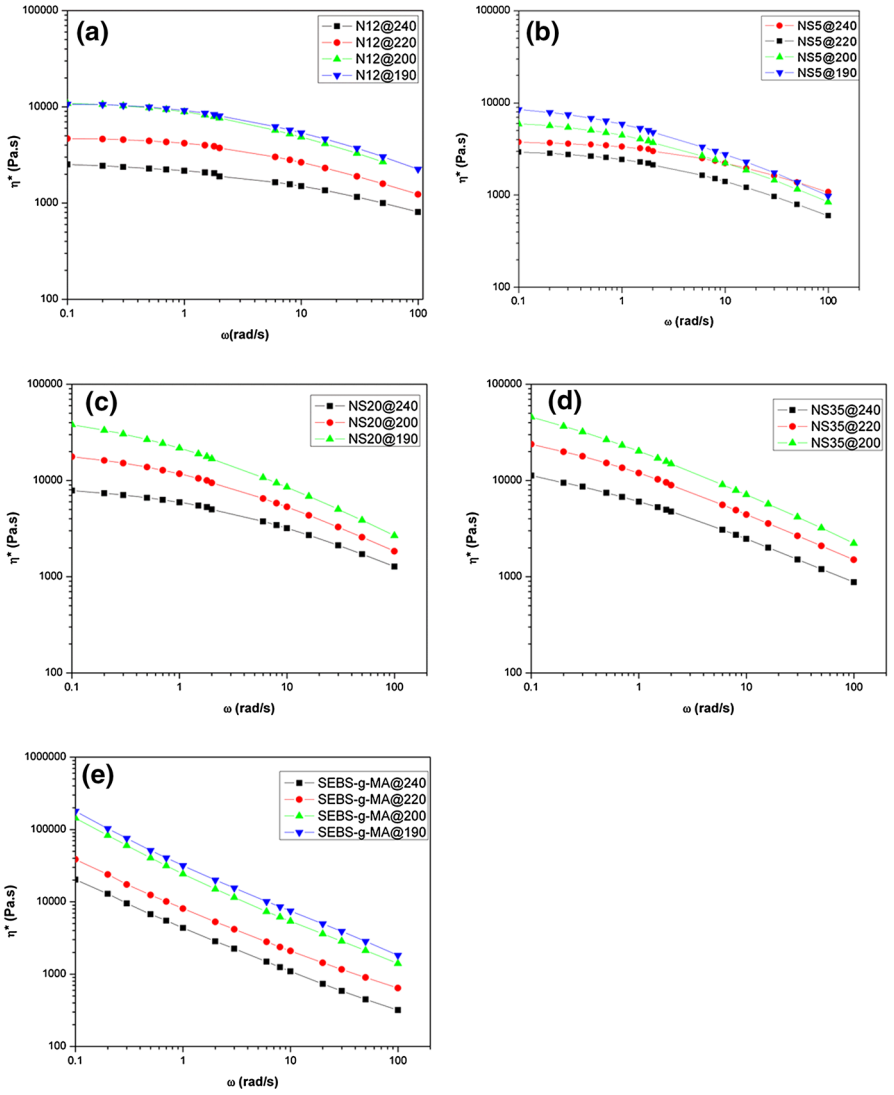

Fig. 9 Plots of complex viscosity vs frequency at different temperature (190–240 °C) for **a** N12, **b** NS10, **c** NS20, **d** NS35, and **e** SEBS-*g*-MA

the polymeric chains could open easily which provides less hindrance to the flow of the melt.

Data of storage modulus at three different temperatures (200, 220, 240 °C) are used to study the applicability of TTS. To check the need of vertical shift factor, b_T, which is the density ratio at reference temperature and temperature of experiment, Cole–Cole plots of modulus (Han Plot, G' vs G'') are used (Fig. 10a–e). Figure 10a–d shows temperature-independent behaviour of the Cole–Cole plot of modulus of PA12, NS10, NS20, and NS35 which has removed the need of vertical shift factor for TTS. In

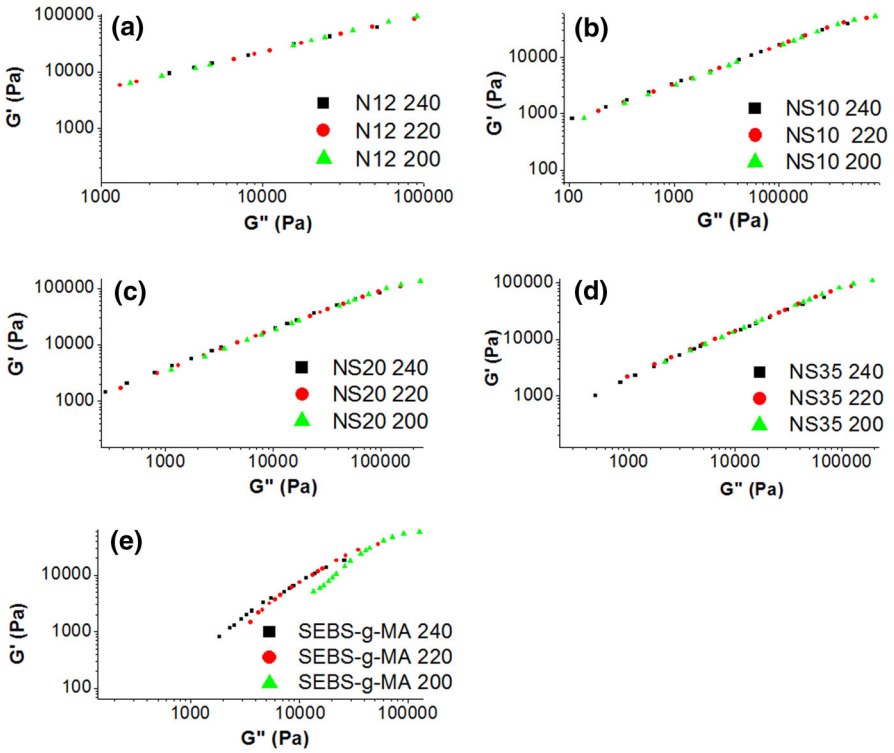

Fig. 10 Cole–Cole plots of modulus at different temperature (200, 220, 240 °C) for **a** N12, **b** NS10, **c** NS20, **d** NS35, and **e** SEBS-*g*-MA

contrast, SEBS-*g*-MA fails the TTS as it shows temperature-dependent Cole–Cole plot of modulus (Fig. 10e). The phase-separated structure and inhomogeneity in the SEBS-*g*-MA copolymer are responsible for this failure [30].

With the help of this concept, one can generate a master curve of rheological data over wide ranges of time and temperature compared to the values of original data. Master curves can be constructed using Williams, Landel, Ferry (WLF) equation, Eq. (5), which relates a shift in temperature with a shift in time:

$$\ln a_{\mathrm{T}} = \frac{-C_1(T - T_0)}{C_2 + (T - T_0)}, \tag{6}$$

where a_{T} is the horizontal shift factor at temperature T, T_0 the reference temperature to which the data are shifted, and C_1 and C_2 the constants derived from curve fitting.

The WLF equation generally holds good if experiments are carried out in the temperature range of Tg to Tg + 100 °C for amorphous polymers. As PA12 is a semicrystalline polymer and the data were generated at 200–240 °C (this temperature is out of range of Tg and Tg +100 °C of PA12), TTS master curves in this case are not well in argument with the WLF equation. Due to this, attempt was made to fit TTS using Arrhenius equation, Eq. (7):

$$\ln a_T = \frac{-E_a}{R}\left(\frac{1}{T} - \frac{1}{T_0}\right), \tag{7}$$

where a_T is the horizontal shift factor at temperature T, R the universal gas constant, and E_a the activation energy for flow at temperature T.

Figure 11a–c shows the representative TTS master curves of PA12, NS10, and SEBS-*g*-MA, respectively, at a reference temperature of 220 °C. It appears to indicate that TTS holds for PA12 and SEBS-*g*-MA but not for the blend. However, more accurate TTS validity was shown by van Gurp plots (Fig. 12a–d). An approach for the verification of TTS was presented by van Gurp and Palmen (1998). They have found that TTS holds only if the plots of measured phase angle (δ) versus the corresponding absolute value of complex shear modulus |(G^*)| merge into a common line [26].

From Fig. 12a, it can be noted that adjacent curves at different temperatures for PA12 are merged into one, hence PA12 follows TTS behaviour. But SEBS-*g*-MA does not follow TTS from van Gurp–Palmen plots and so are the blends (NS10, NS20, and NS35), Fig. 12b–d. The reason of TTS failure in the blends is the microstructural changes and change in the interfacial tension with temperature and the temperature-dependent rheology of SEBS-*g*-MA.

The results obtained are fitted into Arrhenius equation to determine activation energy for flow, Table 2. The activation energies for PA12 (87.9 kJ/mol) and SEBS-*g*-MA (113.2 kJ/mol) phases are quite different which may be responsible for

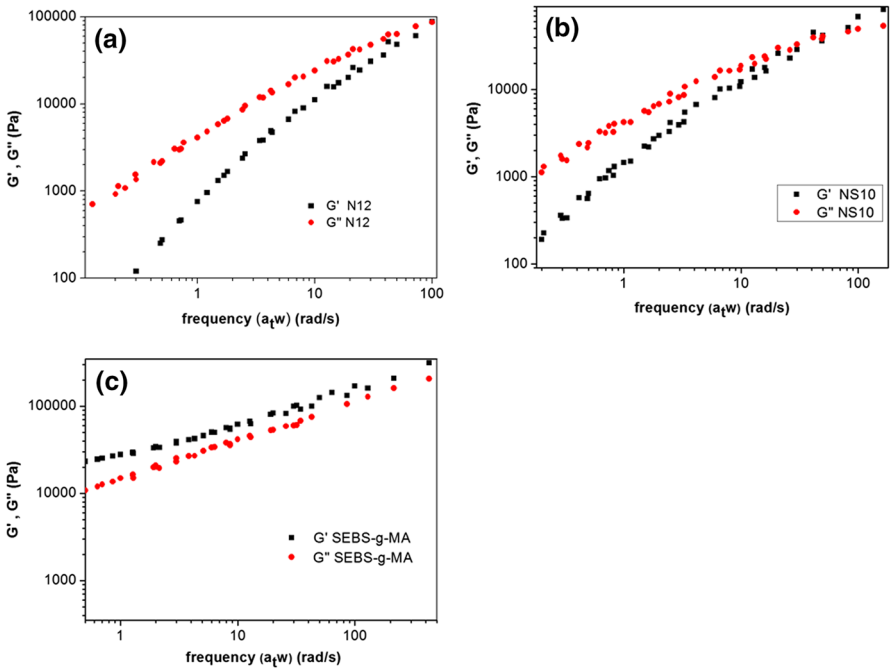

Fig. 11 TTS master curves for **a** N12, **b** NS10, (**c**) SEBS-*g*-MA

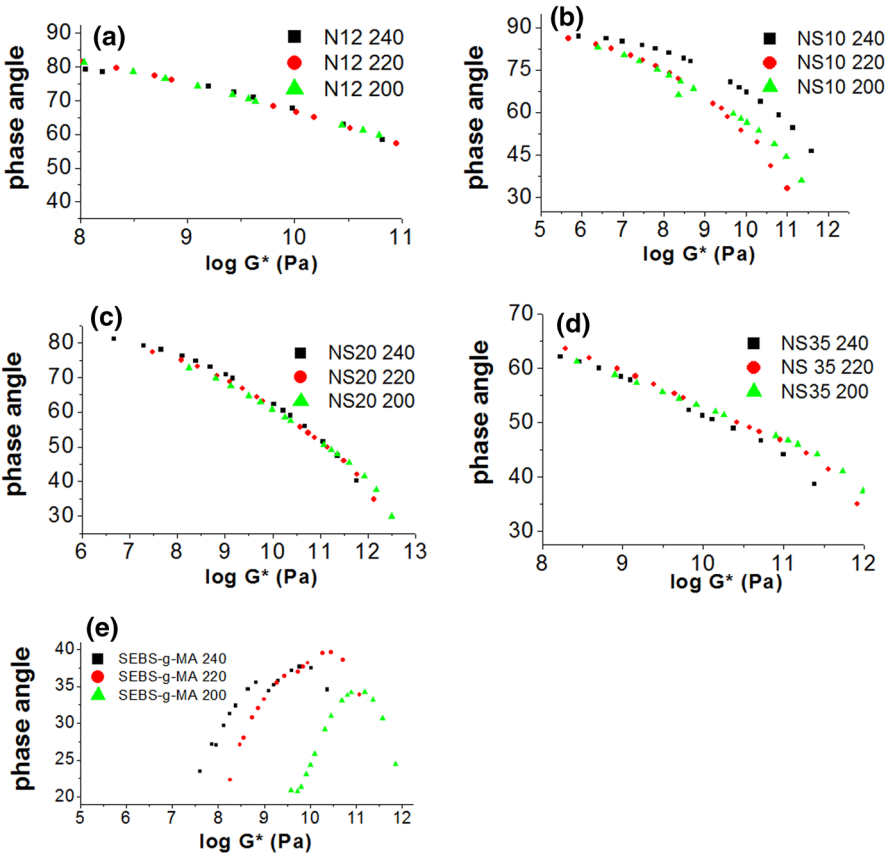

Fig. 12 van Gurp plots at different temperatures different temperature (200, 220, 240 °C) for **a** N12, **b** NS10, **c** NS20, (**d**) NS35, and **e** SEBS-*g*-MA

Table 2 Values of horizontal shift factor (a_t) and Arrhenius activation energy for N12, NS10, NS20, and SEBS-*g*-MA

Sample	a_t			Activation energy (kJ/mol)
	240 °C	220 °C	200 °C	
N12	0.42	1.00	2.40	87.89
NS10	0.42	1.00	2.70	92.9
NS20	0.11	0.36	1.00	109.6
SEBS-*g*-MA	0.31	1.00	2.90	113.24

failure of PA12/SEBS-*g*-MA blends for the TTS behaviour. It can be pointed out that good superposition of rheological data and following the Arrhenius equation are not the only factors to define applicability of TTS; however, van Gurp plots are also used to assess TTS validity [41].

Conclusions

The complex viscosity of the PA12 matrix increased with increasing SEBS-*g*-MA content varying from 5 to 50 wt% due to the grafting reaction between polar groups of PA12 and MA of SEBS-*g*-MA which impede the motion of PA12 polymer chains. Both the storage and loss moduli increased with frequency and SEBS-*g*-MA content. A more sharp increase in storage modulus is observed with increasing SEBS-*g*-MA content which can be considered as solid-like behaviour of the blends. The crossover frequency (ω_x) approached to lower frequency values with increase in SEBS-*g*-MA concentration. Thus, relaxation time increased with higher SEBS-*g*-MA content due to increased restriction imposed by SEBS-*g*-MA. The damping factor, tan δ (G''/G'), decreased and became flatter with increase in frequency and SEBS-*g*-MA concentration as a consequence of elastic nature and occurrence of gel point with 50 % of SEBS-*g*-MA. SEBS-*g*-MA shows typical characteristic rheological behaviour because of its microphase-separated structure and heterogeneity. The complex viscosity η^* decreased with increasing temperature because of enhanced thermal motion and less entanglement density at higher temperature. Failure of TTS in case of SEBS-*g*-MA and blend compositions implies some extent of immiscibility even after improvement in blend compatibility in presence of MA which generates grafting reaction. Cole–Cole plot of modulus showed an enhancement in the solid-like behaviour with increasing concentration of SEBS-*g*-MA. Morphological changes such as size, uniformity, and interparticle distance influenced the rheological properties of the blends. The increase in elastic properties with the addition of SEBS-*g*-MA implies enhanced toughness of the blends.

Acknowledgments We acknowledge the financial support of Council of Scientific & Industrial Research, India, French embassy in India and Ecole des Mines d'Ales, France. Authors are thankful to all the laboratory members and Mr. Marc Longerey for their generous help and support. Author especially thanks to Mr. Belkacem Otazaghine for his helpful assistance and discussions.

References

1. Xanthos M (1992) Reactive extrusion. Hanser, Munich
2. Baker WE, Scott CE, Hu GH (2001) Reactive polymer blending. Hanser, Munich
3. Folkes MJ, Hope PS (1993) Polymer blends and alloys. Chapman & Hall, London
4. Jeon HK, Zhang J, Macosko CW (2005) Premade vs. reactively formed compatibilizers for PMMA/PS melt blends. Polymer 46 (26):12422–12429. doi:10.1016/j.polymer.2005.10.125
5. O'Brien CP, Rice JK, Dadmun MD (2004) Reactive processing with difunctional oligomers to compatibilize polymer blends. Eur Polym J 40(7):1515–1523. doi:10.1016/j.eurpolymj.2004.01.023
6. Kohan MI (1995) Nylon plastics handbook. Hanser, Munich
7. Wang W, Cao Y, Wang J, Zheng Q (2009) Rheological characterization and morphology of nylon 1212/functional elastomer blends. J Appl Polym Sci 112:953–962
8. Kumar S, Ramanaiah BV, Maiti SN (2006) Effect of maleation on polyamide-6/EPDM-G-MAH Blends. Soft Mater 4(1):85–100
9. Huang JJ, Keskkula H, Paul DR (2006) Comparison of the toughening behavior of nylon 6 versus an amorphous polyamide using various maleated elastomers. Polymer 47:639–651. doi:10.1016/j.polymer.2005.11.088
10. Jha A, Bhowmick AK (1998) Thermal degradation and ageing behaviour of novel thermoplastic elastomeric nylon-6/acrylate rubber reactive blends. Polym Degrad Stab 62(3):575–586. doi:10.1016/S0141-3910(98)00044-5

11. Kumar CR, Nair SV, George KE, Oommen Z, Thomas S (2003) Blends of nylon/acrylonitrile butadiene rubber: effects of blend ratio, dynamic vulcanization and reactive compatibilization on rheology and extrudate morphology. Polym Eng Sci 43(9):1555–1565. doi:10.1002/pen.10131
12. Wang X, Li H (2001) Compatibilizing effect of ethylene–vinyl acetate–acrylic acid copolymer on nylon 6/ethylene–vinyl acetate copolymer blended system: mechanical properties, morphology and rheology. J Mater Sci 36(22):5465–5473. doi:10.1023/a:1012437832479
13. Utracki LA, Kamal MR (1982) Melt rheology of polymer blends. Polym Eng Sci 22(2):96–114. doi:10.1002/pen.760220211
14. Aoki Y, Watanabe M (1992) Morphological, thermal, and rheological properties of nylon/acrylonitrile-butadiene-styrene alloys. Polym Eng Sci 32(13):878–885. doi:10.1002/pen.760321307
15. Utracki LA (2002) Polymer alloy and blends. Hanser, New York
16. Babbar I, Mathur GN (1994) Rheological properties of blends of polycarbonate with poly(acrylonitrile-butadiene-styrene). Polymer 35(12):2631–2635. doi:10.1016/0032-3861(94)90391-3
17. Park SJ, Kim BK, Jeong HM (1990) Morphological, thermal and rheological properties of the blends polypropylene/nylon-6, polypropylene/nylon-6/(maleic anhydride-*g*-polypropylene) and (maleic anhydride-*g*-polypropylene)/nylon-6. Eur Polym J 26(2):131–136. doi:10.1016/0014-3057(90)90176-5
18. Araújo EM, Hage E Jr, Carvalho AJF (2003) Morphological, mechanical and rheological properties of nylon 6/acrylonitrile-butadiene-styrene blends compatibilized with MMA/MA copolymers. J Mater Sci 38(17):3515–3520. doi:10.1023/a:1025648508152
19. Jafari SH, Pötschke P, Stephan M, Warth H, Alberts H (2002) Multicomponent blends based on polyamide 6 and styrenic polymers : morphology and melt rheology. Polymer 43(25):6985–6992. doi:10.1016/S0032-3861(02)00614-6
20. Paul DR, Newman S (1978) Polymer blends. Academic, New York
21. Manson JA, Sperling LH (1976) Polymer blends and composites. Plenum, New York
22. Lenderman H (1943) Elastic and creep properties of filamentous materials and other high polymers. Textile Foundation, Wisconsin, Madison
23. Williams ML, Landel RF, Ferry JD (1955) Temperature dependence of relaxation mechanisms in amorphous polymers and other glass forming liquids. J Am Chem Soc 77:3701–3707
24. Seitz JT, Balazs CF (1968) Application of time–temperature superposition principle to long term engineering properties of plastic materials. Polym Eng Sci 8(2):151–160. doi:10.1002/pen.760080211
25. Ferry JD (1980) Viscoelastic properties of polymers. Wiley, New York
26. Marnix VG, Palmen J (1998) Time–temperature superposition for polymeric blends. Rheol Bull 67:5–8
27. Jose S, Thomas PS, Thomas S, Karger-Kocsis J (2006) Thermal and crystallisation behaviours of blends of polyamide 12 with styrene–ethylene/butylene–styrene rubbers. Polymer 47(18):6328–6336
28. Carreau PJ (1968) Rheological equations from molecular network theories. Doctoral dissertation, University of Wisconsin, Madison, Wisconsin
29. Rinawa K, Maiti SN, Sonnier R, Cuesta J-ML (2014) Influence of microstructure and flexibility of maleated styrene-b-(ethylene-*co*-butylene)-b-styrene rubber on the mechanical properties of polyamide 12. Polym Bull 71(5):1131–1152. doi:10.1007/s00289-014-1115-4
30. Mathew I, George KE, Francis DJ (1994) Viscous and elastic behaviour of SEBS triblock copolymer. Die Angewandte Makromolekulare Chemie 217:51–59
31. Nandan B, Kandpal LD, Mathur GN (2004) Poly(ether ether ketone)/poly(aryl ether sulfone) blends: melt rheological behavior. J Polym Sci Part B Polym Phys 42(8):1548–1563. doi:10.1002/polb.20039
32. Han CD, Kim JK (1993) On the use of time–temperature superposition in multicomponent/multiphase polymer systems. Polymer 34(12):2533–2539. doi:10.1016/0032-3861(93)90585-X
33. Han CD, Chuang H-K (1985) Criteria for rheological compatibility of polymer blends. J Appl Polym Sci 30(11):4431–4454. doi:10.1002/app.1985.070301118
34. Han CD, Yang H-H (1987) Rheological behavior of compatible polymer blends. I. Blends of poly(styrene-*co*-acrylonitrile) and poly(ε-caprolactone). J Appl Polym Sci 33(4):1199–1220. doi:10.1002/app.1987.070330412
35. Lim S-K, Hong E-P, Song Y-H, Park BJ, Choi HJ, Chin I-J (2010) Preparation and interaction characteristics of exfoliated ABS/organoclay nanocomposite. Polym Eng Sci 50(3):504–512. doi:10.1002/pen.21551
36. Hansen CM (2007) Hansen solubility parameters: a user's handbook, 2nd edn. CRC Press, Boca Raton

37. Wang X, Feng W, Li H, Ruckenstein E (2002) Optimum toughening via a bicontinuous blending: toughening of PPO with SEBS and SEBS-*g*-maleic anhydride. Polymer 43(1):37–43. doi:10.1016/S0032-3861(01)00601-2
38. Joshi M, Butola BS, Simon G, Kukaleva N (2006) Rheological and viscoelastic behaviour of HDPE/octamethyl-POSS nanocomposites. Macromolecules 39:1839–1849
39. Reichert P, Hoffmann B, Bock T, Thomann R, Mülhaupt R, Friedrich C (2001) Morphological stability of poly(propylene) nanocomposites. Macromol Rapid Commun 22(7):519–523. doi:10.1002/1521-3927(20010401)22:7<519:aid-marc519>3.0.co;2-w
40. Trinkle S, Friedrich C (2001) Van Gurp–Palmen-plot: a way to characterize polydispersity of linear polymers. Rheol Acta 40:322–328
41. Macaubas PHP, Demarquette NR (2002) Time–temperature superposition principle applicability for blends formed of immiscible polymers. Polym Eng Sci 42:1509–1519